Science of the Total Environment 910 (2024) 168656

Contents lists available at ScienceDirect

Science of the Total Environment

journal homepage: www.elsevier.com/locate/scitotenv

Significant changes in cloud radiative effects over Southwestern United States during the COVID-19 flight reduction period

Jingyu Wang [a,*], Yun Lin [b,*], Xianfeng Wang [c,d], Yu Gu [b], Steve Hung-Lam Yim [c,d,e]

[a] National Institute of Education, Nanyang Technological University, Singapore 637616, Singapore
[b] Joint Institute for Regional Earth System Science and Engineering, Department of Atmospheric and Oceanic Sciences, University of California, Los Angeles, Los Angeles, CA 722805, USA
[c] Earth Observatory of Singapore, Nanyang Technological University, Singapore 639798, Singapore
[d] Asian School of the Environment, Nanyang Technological University, Singapore 639798, Singapore
[e] Lee Kong Chian School of Medicine, Nanyang Technological University, Singapore 639798, Singapore

HIGHLIGHTS

- Southwestern US and Western Europe showed distinct responses in CRE during COVID-19.
- Changes in SW/LW CRE in southwestern US were caused by the decline in cirrus clouds.
- The reduction in cirrus clouds was jointly caused by abnormal atmosphere and flight reduction.

GRAPHICAL ABSTRACT

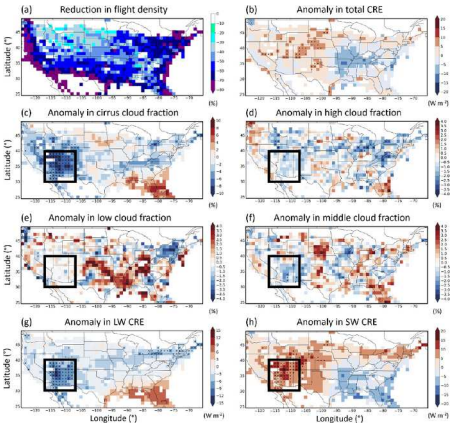

ARTICLE INFO

Editor: Anastasia Paschalidou

Keywords:
COVID-19
Contrail
Flight reduction
Cloud radiative effect
Southwestern US
Aircraft-induced clouds

ABSTRACT

Aircraft-induced clouds (AICs) are one of the most visible anthropogenic atmospheric phenomena, which mimic the natural cirrus clouds and perturb global radiation budget by reducing incoming shortwave (SW) radiation and trapping outgoing longwave (LW) radiation. The COVID-19 pandemic has caused a 70 % global decline in flight numbers from mid-March to October 2020, which provided a unique opportunity to examine the climatic impact of AICs. Among various regions, Western Europe and the Contiguous United States experienced the most substantial reduction in air traffic during the COVID-19 pandemic. Interestingly, only the Southwestern United States demonstrated a significant decrease in cirrus clouds, leading to notable changes in shortwave (SW) and longwave (LW) cloud radiative effects. Such changes were likely due to the reduction in AICs. However, further investigations indicated that this region also experienced abnormal high pressure and low relative humidity in the middle and upper atmosphere, resulting in unusual subsidence and dryness that prohibit the formation and

* Corresponding authors.
E-mail addresses: jingyu.wang@nie.edu.sg (J. Wang), yunlin@ucla.edu (Y. Lin).

https://doi.org/10.1016/j.scitotenv.2023.168656
Received 2 September 2023; Received in revised form 13 November 2023; Accepted 15 November 2023
Available online 20 November 2023

maintenance of cirrus cloud. While it remains challenging to quantify the exact climatic impact of reduced AICs, the remarkable anomalies documented in this study provide valuable observational benchmark for future modelling studies of the climatic impact AICs.

1. Introduction

Contrails form in aircraft trailing plumes as a result of mixing between the warm and moist engine exhaust and the cold environment. The localized surge in water vapor can increase the humidity, leading to the condensation and subsequent freezing of small liquid droplets (Schumann, 2005). These form the visible line-shaped cirrus clouds that last from a few seconds to 17 h (Minnis et al., 1998) at 8–13 km in altitude (Kärcher, 2018). It has been recognized that aviation activities have the potential to augment cirrus cloud formation (Boucher, 1999). The line-shaped contrails, together with the irregularly shaped cirrus that arises from aviation activities (Burkhardt and Kärcher, 2011), have been referred to as aircraft-induced clouds (AICs) (Kärcher, 2018). Most AICs are optically thin and consist of relatively small particles, therefore they tend to reduce incoming daytime solar radiation and trap outgoing infrared radiation at night, thus may induce changes to the temperature structure in the lower atmosphere (Travis et al., 2002; Meerkötter et al., 1999; Duda et al., 2001). In the context of large uncertainties in the anthropogenic impact on future climate change (Liu et al., 2018), it is important to understand the contribution of increasing air traffic, which is projected to quadrupled in 2050 relative to 2006 (Wilkerson et al., 2010). AICs have strong cloud radiative effect (CRE) associated with air traffic that is comparable in magnitude to the CO_2 accumulation from aviation (Burkhardt and Kärcher, 2011; Kärcher, 2018). Therefore, researchers have been working on the assessment of the AICs CRE and their possible large-scale climatic impact for decades (Matthews and Kellogg, 1971; Graßl, 1990; Schumann and Wendling, 1990; Schumann and Graf, 2013). Consensus has been reached that AICs have stronger longwave (LW) CRE than shortwave (SW), resulting in a positive net CRE at top-of-atmosphere (TOA; Lee et al., 2021).

Line-shaped AICs are relatively easy to distinguish from natural cirrus clouds both visually and by satellite observations (Minnis et al., 2013) because of their linear pattern. Based on numerical models with the parameterization capability of simulating line-shaped contrails (Minnis et al., 1998; Myhre and Stordal, 2001; Marquart et al., 2003), as well as the satellite observations, the global CRE of contrails has been estimated to be 10 mW m^{-2} with the uncertainty ranging from 5 to 30 mW m^{-2} by the Intergovernmental Panel on Climate Change (IPCC) (Boucher et al., 2013), depending on the simulation year and assumed contrail properties (e.g., optical depth [Kärcher et al., 2010]). In comparison, the detection and observation of irregularly shaped cirrus that arises from aviation activities is more difficult owing to its similarity to natural cirrus (Heymsfield et al., 2010). With the best estimate of global AIC CRE of 40 mW m^{-2}, the global CRE of AICs is 50 mW m^{-2} (Boucher et al., 2013). Relative to 2006, the global AIC CRE is projected to increase to 160 mW m^{-2} or even 180 mW m^{-2} by 2050 along with the projected increase in air traffic volume (Bock and Burkhardt, 2019).

It is important to note that those estimates greatly rely on the model simulations, therefore the uncertainty in the underlying mechanisms and their parameterization in models may cause large uncertainty in the CRE of AIC, which hinders the development of mitigation solutions to reduce the climatic impact of aviation activities. Although there were global estimates generated by jointing the extrapolated local air traffic and satellite observations together with the model simulation (Schumann and Graf, 2013; Spangenberg et al., 2013; Lee et al., 2021), the robust estimates of the CRE of AICs are still missing because of the lack of observational evidence (Kärcher, 2018).

Anomalous aviation events provide unique opportunities to examine the climatic impact of contrails from the observational perspective. During the three-day grounding of all commercial aircrafts after 11 September 2001, studies reported an average daily temperature range (DTR) increase of 1.8 °C in the United States, and a contribution by the reduced contrails was proposed (Travis et al., 2002; Travis et al., 2004). However, due to the short duration of the disruption, the impact of contrail reduction on the DTR change remains debatable. The reported DTR anomaly was suggested within the range of natural variability with a concurrent low-cloud anomaly also contributing (Hong et al., 2008). In contrast, the long-lasting COVID-19 pandemic, which began in mid-March 2020 and continued through late 2021, has produced a remarkable global reduction in flight numbers (Chen, 2020) by 70 % compared to 2019 as shown in Fig. 1a. This extensive flight reduction provides an unprecedented opportunity to explore the climatic impact of contrails based on observations (Digby et al., 2021; Gettelman et al., 2021; Li and Groß, 2021; Quaas et al., 2021; Schumann et al., 2021a, 2021b; Meijer et al., 2022; Voigt et al., 2022; Duda et al., 2023).

2. Data and methods

2.1. Air traffic observations

National Oceanic and Atmospheric Administration (NOAA) Meteorological Assimilation Data Ingest System (MADIS) Aircraft Based Observation (ABO) provides real-time meteorological observations obtained from airlines across the globe (https://madis.ncep.noaa.gov/madis_acars.shtml). The location information of aircrafts is recorded using airborne sensors every 10 min. The point-based records are mapped to a global grid with 1° by 1° resolution. Note that although the meteorological sensors were not equipped on all aircrafts, the flight track information collected by MADIS ABO is still considered representative of the global flight distribution. Based on this dataset, we used the following criteria to identify the most affected grid elements: 1) the top 5th percentile flight density of the globe during the pre-pandemic period (i.e., >1584 flight overpasses per month), and 2) the percentage of reduction during the pandemic relative to the pre-pandemic exceeding 25 % (>13 overpasses reduced per day). By comparing the April–October global flight density between the past 4 years (2016–2019; Fig. 1b) and 2020 (Fig. 1c), two regions with the most significant reduction stood out, namely the Contiguous United States (CONUS) and the Western Europe (Fig. 1d). Two domains (25°–50°N, 66°–125°W) and (41°–59°N, 10°W–20°E) were selected to roughly enclose the two regions. The domain average reduction in flight number was 6165 (−56 %) for CONUS, and 1193 (−59 %) over Western Europe.

2.2. Satellite observations of cloud radiative effects, cloud fractions, and cloud properties

Clouds and the Earth's Radiant Energy System (CERES) Energy Balanced and Filled (EBAF) Edition 4.1 (CERES_EBAF_Edition4.1; available at https://asdc.larc.nasa.gov/project/CERES/CERES_EBAF_Edition4.1) is a National Aeronautics and Space Administration (NASA) dataset that provides detailed information of Earth's radiation budget (global monthly data with 1° × 1° resolution). This dataset is produced based on CERES Scanner instrument suite on both the Terra and Aqua platforms, which measure the solar and thermal radiation at both top-of-atmosphere (TOA) and surface, providing a comprehensive view of the energy exchange between Earth and atmosphere. CERES_EBAF_Edition4.1 is an updated version of CERES-EBAF product, which has been widely used for climate research and modelling (Loeb et al., 2018; Doelling, 2019; Dolinar et al., 2019; Zhao et al., 2022). This dataset was used in this study for assessing the monthly climatological

averages of TOA CRE at SW and LW during the COVID-19 flight reduction period. The CRE was defined as the amount of radiative energy that would return to space if there were no clouds (clear sky condition), minus the amount that actually escapes with clouds present (all sky condition). It's important to highlight that SW CRE typically leads to cooling (negative sign), while LW CRE causes warming (positive sign) at TOA. Moreover, the sensitivity to changes in cloud fraction is higher for SW/LW CREs rather than the total CRE.

The MODIS Level 3 Monthly Atmosphere Gridded product developed by NASA Goddard Space Flight Center is available monthly at global scale with 1° × 1° resolution (Platnick et al., 2015; available at https://ladsweb.modaps.eosdis.nasa.gov/archive/allData/61/MYD08_M3/), which contains important cloud properties including cirrus cloud fraction, optical thickness, effective radius, and water path for liquid/ice cloud. Mace et al. (2004) conducted a comprehensive evaluation of MODIS cirrus products in comparison to ground-based observations, revealing a significant alignment between the two platforms. There are two such datasets based on the data collected from the Terra (MOD08_M3) and Aqua (MYD08_M3) platforms. In this study, only the MYD08_M3 data were used to display the results as the major conclusions were not affected by the differences between the two datasets.

To examine if only the cirrus cloud fractions were disturbed during the COVID-19 related flight reduction, the monthly cloud fraction data were obtained from the Multi-angle Imaging SpectroRadiometer (MISR) Cloud Fraction by Altitude (CFbA) Product (Moroney et al., 2019; available at https://asdc.larc.nasa.gov/data/MISR/MIL3MCFA.001/).

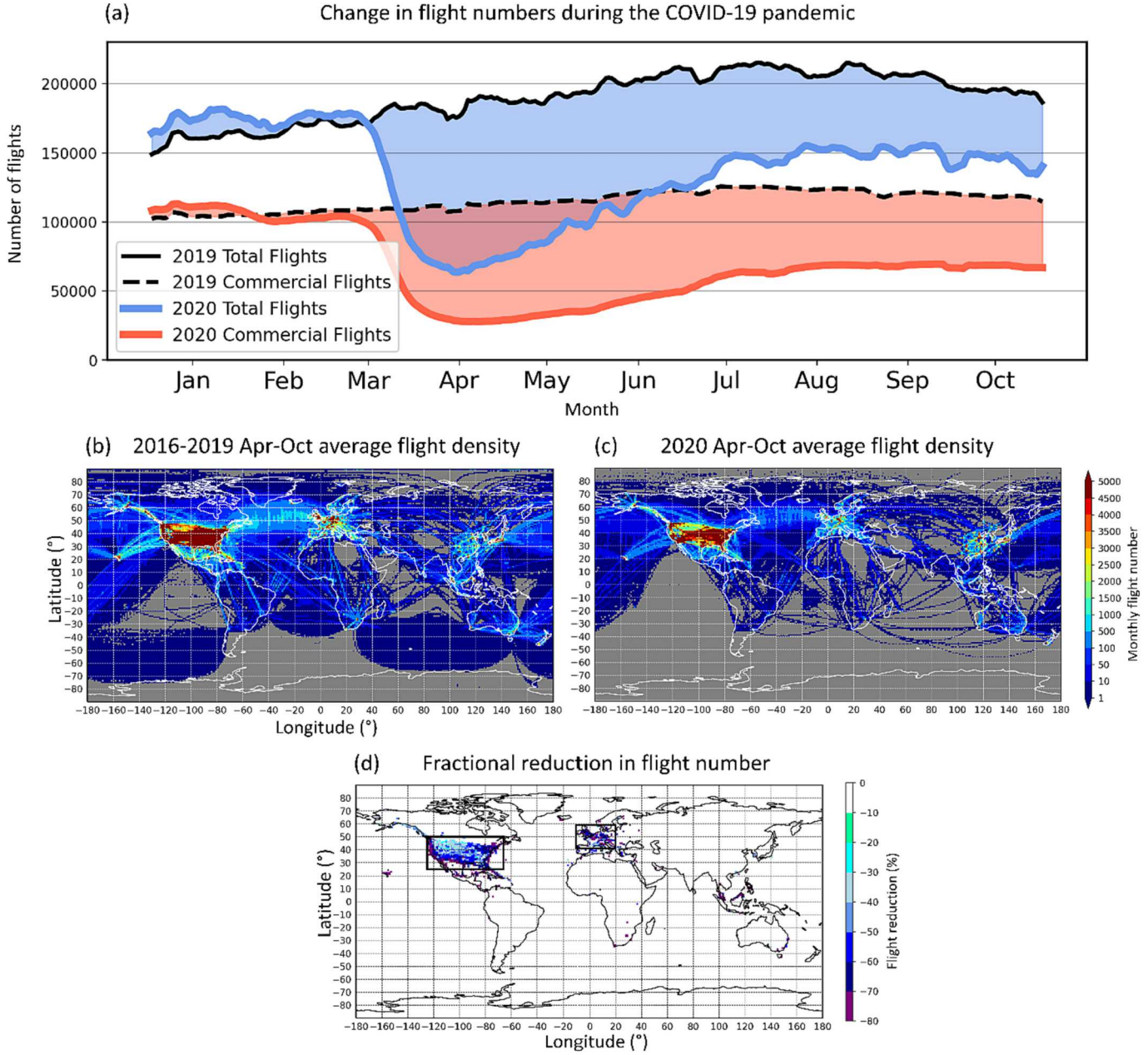

Fig. 1. (a) 7-day moving averages of total flight and commercial flight numbers for 2019 and 2020, data obtained from FilghtRadar24 (available at https://www.flightradar24.com/data/statistics). (b) The April–October monthly average flight density during the pre-pandemic period in 2016–2019 (data obtained from MADIS ABO). (c) Similar as (b), but for the pandemic period in 2020. (d) The fractional difference between (b) and (c), where only the most affected grid elements satisfying the following criteria were shown: 1) the top 5th percentile flight density of the globe during the pre-pandemic period, and 2) the percentage of reduction during the pandemic relative to the pre-pandemic exceeding 25 %. The boxed regions indicate areas of interest for CONUS (25°–50°N, 66°–125°W) and Western Europe (41°–59°N, 10°W–20°E).

This product contains the frequency of cloud occurrence separated into different vertical levels (with 500 m interval from surface to 20 km above mean sea level) on a global (0.5° × 0.5° resolution) and monthly basis. This study classifies clouds into three categories based on the height range: low clouds (which have altitudes between 0 and 3.5 km), middle clouds (with heights between 3.5 km and 8 km), and high clouds (with heights between 8 km and the topmost level of the data). To better characterize the cloud presence for each category and avoid the confusion brought by overlapping clouds, the column-maximum cloud fraction was used to represent each grid column at the three designated vertical levels.

2.3. Reanalysis data for the meteorological conditions

Modern-Era Retrospective Analysis for Research and Applications Version 2 (MERRA-2) is an atmospheric reanalysis dataset developed by NASA that employs a recent version of the Goddard Earth Observing System, version 5 data assimilation system (Bosilovich et al., 2015; available at https://gmao.gsfc.nasa.gov/reanalysis/MERRA-2/data_access/). MERRA-2 provides global atmospheric variables at 3-hourly intervals and 0.5° × 0.625° spatial resolution, with 72 vertical pressure levels ranging from the surface to TOA. MERRA-2 has been proven competent in representing the large-scale atmospheric circulation worldwide (Gelaro et al., 2017), therefore the monthly MERRA-2 data were analyzed in this study to examine the atmospheric background over the regions with the most significant flight reduction.

It is noted that all the flight track data, satellite-based cloud observations, and reanalysis data were collected and analyzed at the monthly scale from April to October (the most substantial flight reduction period before the gradual resumption of air traffic starting from November 2020). The period from 2003 to 2019 was designated as the pre-pandemic period, and it established the historical climate background against which the anomalies during COVID-19 period of 2020 was compared to. All the data were averaged to the coarsest spatial resolution of the MODIS atmospheric product at 1° × 1° resolution.

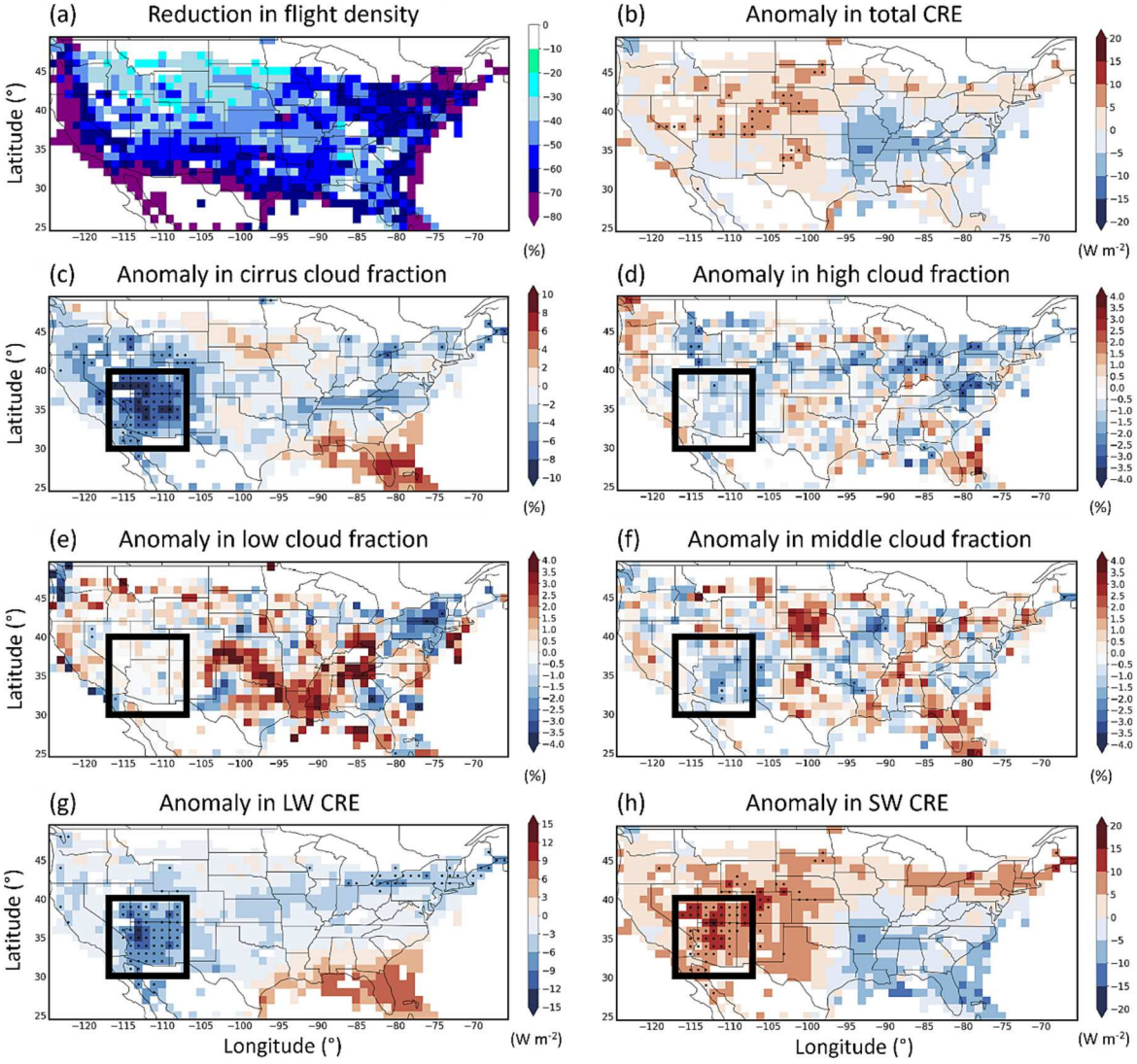

Fig. 2. (a) The April–October 2020 reduction in flight density compared to 2016–2019 average (based on MADIS ABO). The anomalies in (b) total CRE, (c) cirrus, (d) high, (e) low, and (f) middle cloud fractions (based on MODIS), as well as the anomalies in (g) longwave (LW) and (h) shortwave (SW) CREs (based on CERES EBAF). (b-h) are generated by comparing the pandemic period (April–October 2020) with the pre-pandemic climatology (April–October 2003–2019). A grid element whose value higher/lower than the 95th/5th percentile of its historical records is marked with a black dot to indicate significant positive/negative bias. The black box in (c-h) encloses the sub region of interest (30°–40°N, 107°–117°W).

3. Results

3.1. Observed anomalies in CREs and cloud fractions over CONUS during COVID-19

As mentioned in Section 2.1, two regions emerge with the most significant flight reduction. By zooming into the study region of CONUS (Fig. 2a), it is found that the greatest decrease in flights occurs along the east and west coasts, with the northeast and southwest regions following closely behind. In terms of the spatial anomaly in total cloud radiative effect (CRE; Fig. 2b), which is the combination of both LW and SW CREs, the western half is dominated by positive anomalies, while the southeastern part is mostly characterized by negative anomalies, however only the former section has a few significances. It appears that this region's total CRE was not significantly perturbed by the substantial reduction in flight density with a minimal increase (1.6 W m^{-2} vs. 2.0 W m^{-2} nationwide; Fig. 2b). Nonetheless, this could result from a counterbalancing effect between the opposite LW/SW CREs, as well as the varying changes in cloud fractions at different vertical levels.

Based on the MODIS observation, grid elements that experienced the most significant decrease in cirrus cloud fraction are concentrated over the Southwestern US (absolute and relative differences are −6.1 % and − 25.2 % respectively; Fig. 2c). As evidenced by the historical records (2003–2019; Fig. 3a), this specific area (30°–40°N, 107°–117°W) has relatively lower occurrence of circus cloud compared to the rest of CONUS (26.4 % vs. 30.7 % nationwide). Additionally, compared to the entire CONUS, it corresponds to the lowest fractions of high (1.6 % vs. 3.1 % nationwide; Fig. 3b), low (1.3 % vs. 5.9 % nationwide; Fig. 3c) and middle clouds (3.0 % vs. 5.0 % nationwide; Fig. 3d), which is in line with the typical desert climatology (Karl and Koss, 1984). Therefore, it is highly possible that such significant reduction in cirrus cloud coverage could be caused by the COVID-19 flight reduction.

With the most prominent decrease in cirrus cloud during April–October 2020, no significant anomalies in cloud coverage were observed over Southwestern US at altitude levels of high (−0.6 % vs. -0.5 % nationwide; Fig. 2d), low (−0.1 % vs. -0.3 %; Fig. 2e), and middle (−0.8 % vs. 0.2 %; Fig. 2f). It should be noted that the high cloud coverage defined in this study is based on CFbA product, which includes a wide variety of cloud types (i.e., cirrostratus, cirrocumulus, thin cirrus, and possible AICs, as well as all other cloud types with vertical extension above 8 km). Therefore, the cirrus cloud detected by MODIS (Fig. 2c and 3a) is only a subset of CFbA high cloud (Fig. 2d and 3b).

As revealed in previous studies (e.g., Minnis et al., 2013), both AICs and thin cirrus clouds are SW reflective and trap outgoing LW radiation emitted by Earth and lower atmosphere. Surprisingly, such signals are well captured in Fig. 2g and h, where the strongest negative/positive anomalies in LW CRE (−6.7 W m^{-2} vs. -2.5 W m^{-2} nationwide) and SW CRE (8.3 W m^{-2} vs. 4.5 W m^{-2} nationwide) are observed over Southwestern US, with majority of the region (64 % and 63 % respectively) passing significance test. As expected earlier, the marginal rise in total CRE over the Southwestern US is quite misleading as it masks the substantial contrasting changes in LW and SW CREs.

3.2. Observed anomalies in cloud properties during COVID-19

As suggested in previous studies (e.g., Dong et al., 2000, 2014), the drastic changes in CREs and cloud fractions should also be reflected in cloud properties including cloud optical thickness (COT), liquid/ice water path (LWP/IWP), and effective radius (Re) of cloud particles. Fig. 4 illustrates the anomalies in cloud properties observed by MODIS, and apparently only the ice COT was significantly perturbed (−3.8 vs. -0.3 nationwide with 36 % of gird elements within Southwestern US passing significance test; Fig. 4a) in comparison with liquid COT (−0.2 vs. -1.2 nationwide and only 7 % of grid elements passed significance test; Fig. 3b). These results echoed the conclusions in Section 3.1 that only the cirrus cloud (mostly in ice phase) had been significantly impacted during the COVID-19 flight reduction period, while the lower-level clouds (mostly in liquid phase) were not notably perturbed. It is worth noting that non-aviation activities (i.e., surface emissions) were also greatly reduced during the pandemic, therefore the unchanged lower-level cloud warrants further investigation.

Similar as liquid cloud (Hansen and Travis, 1974; Brenguier et al., 2011), the ice COT can be simply estimated by IWP and R_e using the following approximation (Horváth and Davies, 2007; Wang et al., 2019):

$$COT \approx \frac{3}{4} IWP \Big/ R_e \tag{1}$$

As a result, further investigation is required to identify the primary factor responsible for the observed change in ice COT. As shown in Fig. 4c and d, only significant decrease in IWP was found over Southwestern US, whereas the corresponding R_e remained unchanged (quantitative results are listed in Table 1). The findings suggest that the decrease in IWP has the most significant impact on the altered ice COT during COVID-19. This effect is likely linked to substantial changes

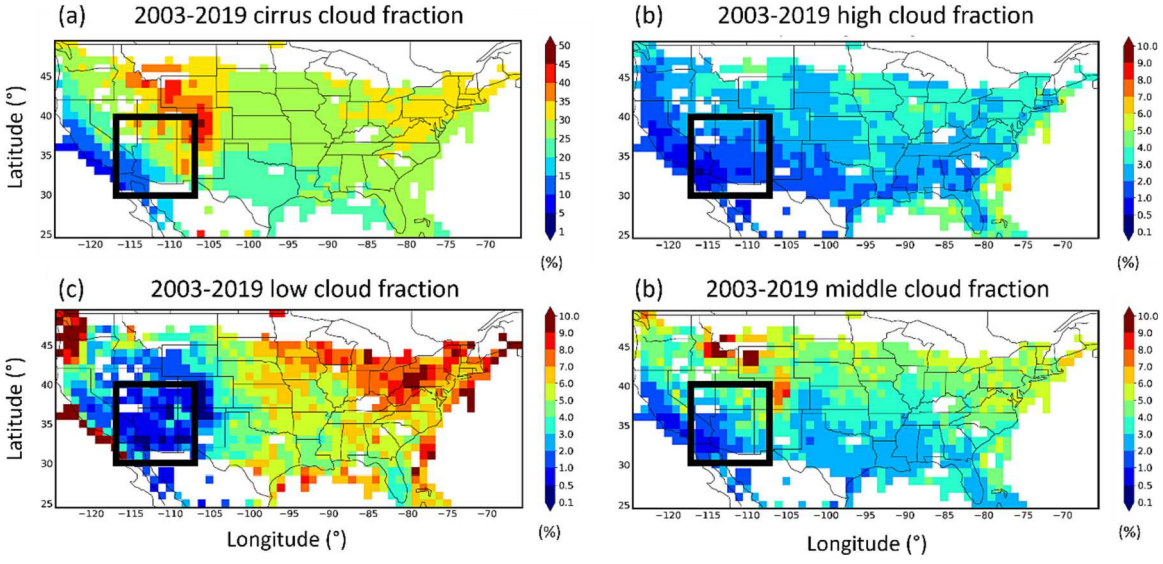

Fig. 3. The climatological conditions of (a) cirrus cloud fraction, (b) high cloud fraction, (c) low cloud fraction, and (d) middle cloud fraction averaged during April–October 2003–2019 (based on MODIS).

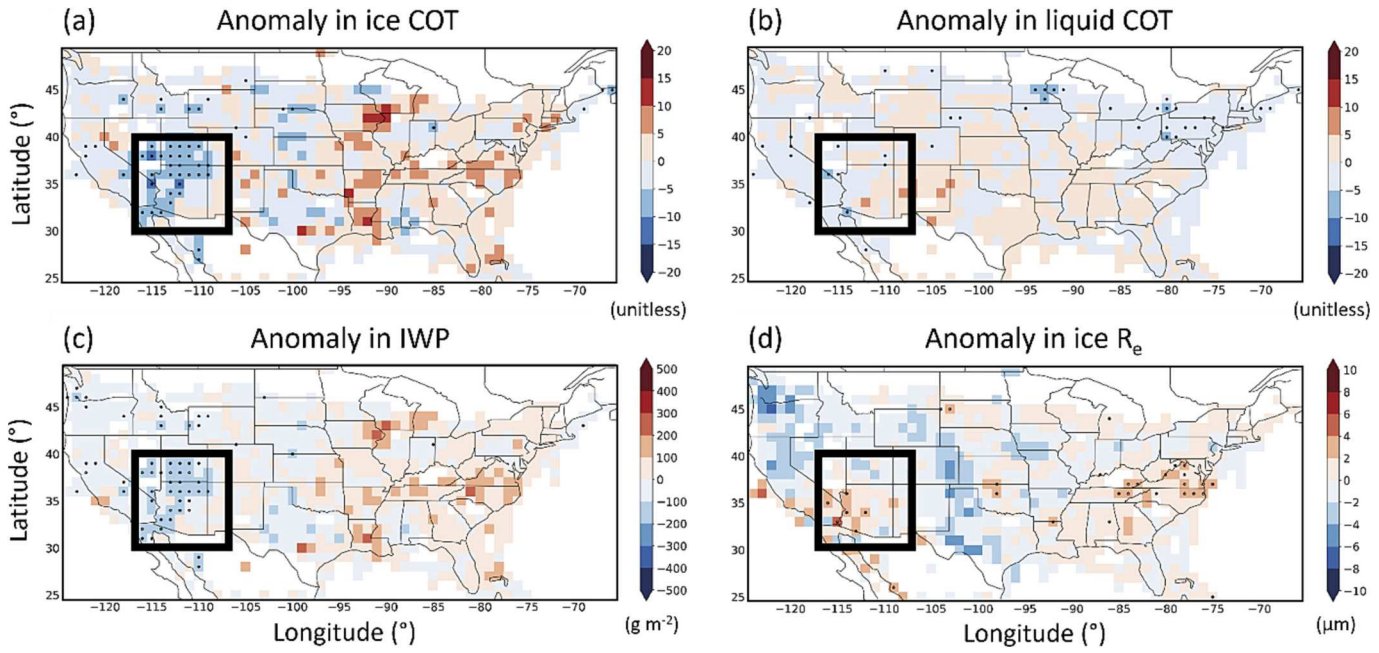

Fig. 4. Same as Fig. 2, but for (a) ice cloud optical thickness (COT), (b) liquid COT, (c) ice water path (IWP), and (d) ice effective radius (R_e) (based on MODIS).

Table 1
Quantitative results of flight numbers, ice COT, IWP, and ice Re over Southwestern US.

	Flight number (#)	Cirrus cloud fraction (%)	Ice COT (unitless)	IWP (g m^{-2})	Ice R_e (μm)
Before 2020	16,688	0.25	17.24	299.67	30.18
2020	6969	0.19	14.25	245.46	30.38

resulting from the sharp decline in flight frequency and subsequent reduction in AICs. However, one cannot solely attribute this to the anthropogenic activities unless the influence of other large-scale atmospheric factors, such as anomalies in moisture and vertical motion profiles can be ruled out. Therefore, further investigation into the potential impact of large-scale factors was performed in the following section.

3.3. Analyses of the potential contributing large-scale factors

Based on the formation mechanism of cirrus (Kärcher, 2017; Zhao et al., 2023), the variables of relative humidity, temperature, geopotential height, and vertical motion were selected and analyzed during the study period. Since the primary cause of the significant decrease in cirrus cloud coverage over the Southwestern US during the pandemic period has been identified as a significant lack of ice cloud water, the moisture availability is therefore the first non-anthropogenic factor to be examined. By averaging the monthly MERRA-2 reanalysis data over the study domain, the 700–500 mb (middle level) and 500–200 mb (high level) relative humidity values (RH) were compared between the pandemic (2020) and pre-pandemic (2003–2019) periods in Fig. 5.

During the beginning months of flight reduction period from April to June, both the 2020 RH at middle and high levels fell within the one standard deviation range of their respective pre-pandemic average, indicating Southwestern US was not abnormally drier than the past. Meanwhile, only minimal numbers of grid elements with significant changes in cirrus cloud fraction and LW/SW CREs were detected during the 3 months. However, during the transition from June to July, when the onset of North American summer monsoon began (Castro et al., 2001, 2012; Mazon et al., 2016), both the middle and upper troposphere experienced drier condition in 2020 than the past, and such deviation persisted until October. In the meanwhile, the number of grid elements with significant changes in cloud properties increased rapidly with SW peaked in August (28 out of 81 total grid elements within southwestern US), and both cirrus cloud fraction and LW peaked in September (38 and 28 respectively). These results reveal the possibility that the significant decrease in circus cloud coverage may not be solely caused by COVID-19 related flight reduction, but is likely governed by the RH anomalies at middle to upper troposphere.

By focusing on the 3 months of monsoon season from July to September, which correspond the largest number of grids that experienced the significant reduction in cirrus cloud fraction, Figs. S1-S3 illustrate the anomalies in cloud properties as compared to their counterparts in April–October (Figs. 2–4). Apparently, the reduction in cirrus cloud fraction, LW CRE, ice COT, and IWP, as well as the increase in SW CRE became more substantial, indicating the 3 months of July–September held a dominant influence over the perturbed atmospheric condition during the flight reduction period. For comparison, the pre-monsoon cloud properties are shown in Figs. S4-S6. Notably, there were no significant changes in cirrus cloud coverage observed across the study area (Fig. S4c). Additionally, the average cirrus cloud coverage during April–June (Fig. S5a) was considerably lower than that during the monsoon period from July to September (Fig. S2a). Meanwhile, there were no significant differences found in ice COT, IWP, or ice R_e. All these findings suggest that the reduction in flights during the COVID-19 period had a more noticeable impact during the monsoon season compared to the pre-monsoon season.

To examine if there exists a climatological drying trend over middle and upper troposphere over southwestern US, Fig. 6a and b show the long-term trend of the two variables (April–October average) over the past two decades. Surprisingly, instead of a drying trend, Southwestern US is becoming moister at middle-upper troposphere. Moreover, it is worth noting that Southwestern US sets the new driest records at both layers in 2020 (red dots). Therefore, the abrupt decrease of RH during the COVID-19 flight reduction period is against the climatological wetting trend and should be considered as abnormal. In addition to the middle and upper troposphere, the drier condition is found throughout the entire atmospheric column (Fig. 6c), which also explains the minimal reduction in low (Fig. 2e) cloud over this region.

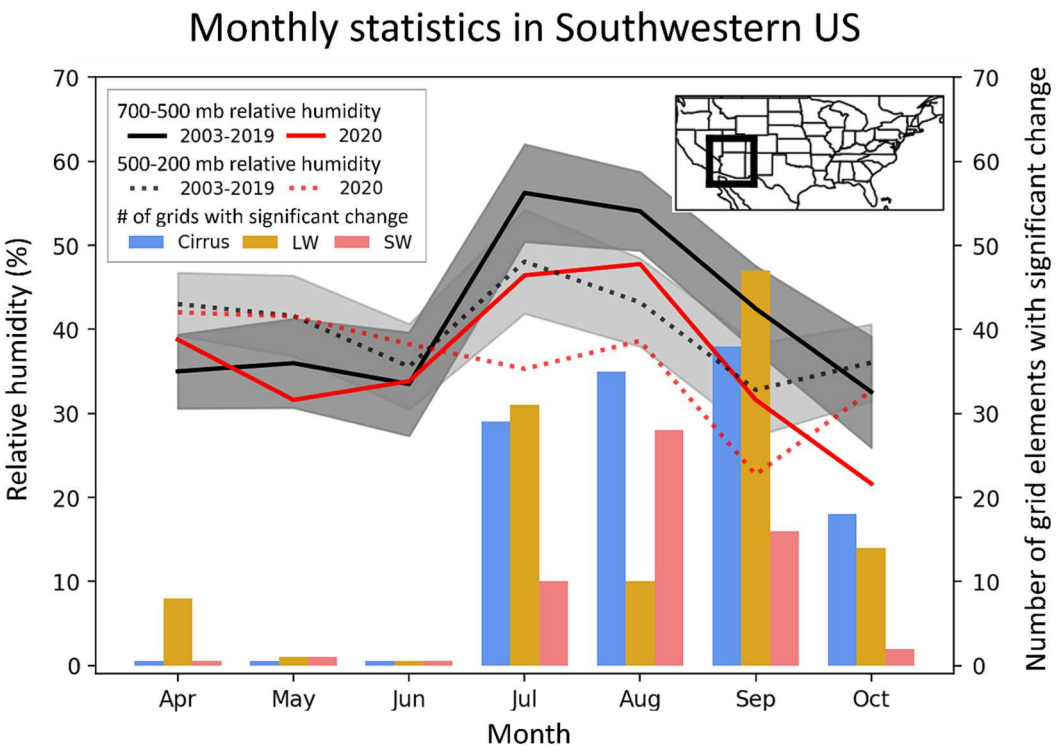

Fig. 5. The comparison between pre-pandemic period (black) and pandemic period (red) in monthly variation of 700–500 mb relative humidity (solid line) and 500–200 mb relative humidity (dash line) over southwestern United States, overlaid by the number of grid elements with significant reduction in cirrus cloud fraction (blue bars), reduction in longwave (LW) CRE (yellow bars), and increase in shortwave (SW) CRE (red bars) (based on MERRA-2). The gray shading around the black solid and dash lines indicates the range of ±1 standard deviation respectively.

In addition to the moisture availability, temperature is another important thermodynamic factor highly related to cloud formation. Based on Fig. 6d–f, a warming trend is observed at both layers in particular to the middle troposphere that shows substantial warming in 2020, and no strong deviation is found in the vertical direction. Therefore, temperature factor may not be as important as RH for this case.

The last large-scale atmospheric factor to be examined is the vertical motion, which is governed by the geopotential height field. A record-setting high geopotential height value is found at both 700 mb (Fig. 6g) and 500 mb (Fig. 6h) in 2020 compared to the pre-pandemic period. Climatologically, the Southwestern US desert is dominated by ascending motion below the tropopause because its surface is exposed to excessive solar heating due to the lack of cloud coverage at various altitudes (Fig. 3). However, the higher-than-normal geopotential heights at 700 mb and 500 mb in 2020 create an environment that favors the large-scale subsidence in middle and upper troposphere. As a result, from 650 mb above, the 2020 vertical motion profile starts to deviate from the historical records, with this deviation growing larger until 500 mb, where the historically ascending motion shifts to descending motion. Then the descending motion reaches its peak at 350 mb, and finally decreases toward 200 mb. The findings reveal that the study region experienced large-scale subsidence in the upper atmosphere during 2020, which also impeded the formation of cirrus clouds.

In summary, the exceptional and unusual dryness and subsidence observed in the middle and upper troposphere show a tendency to suppress the formation cirrus clouds, which coincides with the COVID-19 related flight reduction. Consequently, disentangling the primary cause of the significant decrease in cirrus cloud coverage and the associated substantial changes in CREs becomes challenging due to the intertwined effects of natural variability and anthropogenic influence.

3.4. Analysis of Western Europe

Similar as Fig. 2 for CONUS, analyses in cloud fractions and cloud radiative properties have been conducted over Western Europe as illustrated in Fig. 7. While the spatial extent of the decrease in flights was more constrained, the magnitude of flight reduction in Western Europe (Fig. 7a) is comparable to that observed in CONUS (Fig. 2a). In contrast to the relatively unaffected total CRE over CONUS (Fig. 2b), Western Europe exhibited significant positive anomalies (Fig. 7b). Similar to the Southwestern US, Western Europe experienced a consistent reduction in cirrus cloud fraction but with smaller magnitude (Fig. 7c vs. Fig. 2c). By comparing cloud fractions at various altitudes between the two regions, we observed that both regions maintained relatively stable high (Fig. 2d vs. Fig. 7d) and middle cloud fractions (Fig. 2f vs. Fig. 7f). However, in Western Europe, there was a notable decrease in low cloud fraction (Fig. 7e), whose most significant negative anomalies collocated well with the most pronounced positive anomalies in total CRE (Fig. 7b). The strong correlation in reduced low cloud fraction (Fig. 7e) and increased total CRE (Fig. 7b) suggests that Western Europe's CRE is predominantly influenced by changes in low cloud coverage. By analyzing LW CRE (Fig. 7g) and SW CRE (Fig. 7h), it becomes apparently that both the LW warming effect and the SW cooling effect were notably diminished during the pandemic in the area with the most significant decrease in low cloud fraction. This suggests that the increase in total CRE was primarily driven by the rise in SW CRE (reduced cooling).

Such change is more likely attributable to the absence of thicker and lower cloud formation rather than cirrus cloud. This assertion is further evidenced by the historical records of cloud fractions at various altitudes (Fig. 8). While cirrus cloud was commonly observed over Western Europe (Fig. 8a), it is apparent that this region consistently featured a higher proportion of low cloud (Fig. 8c) compared to high (Fig. 8b) and middle cloud (Fig. 8d). As a result, this dominance of low cloud played a

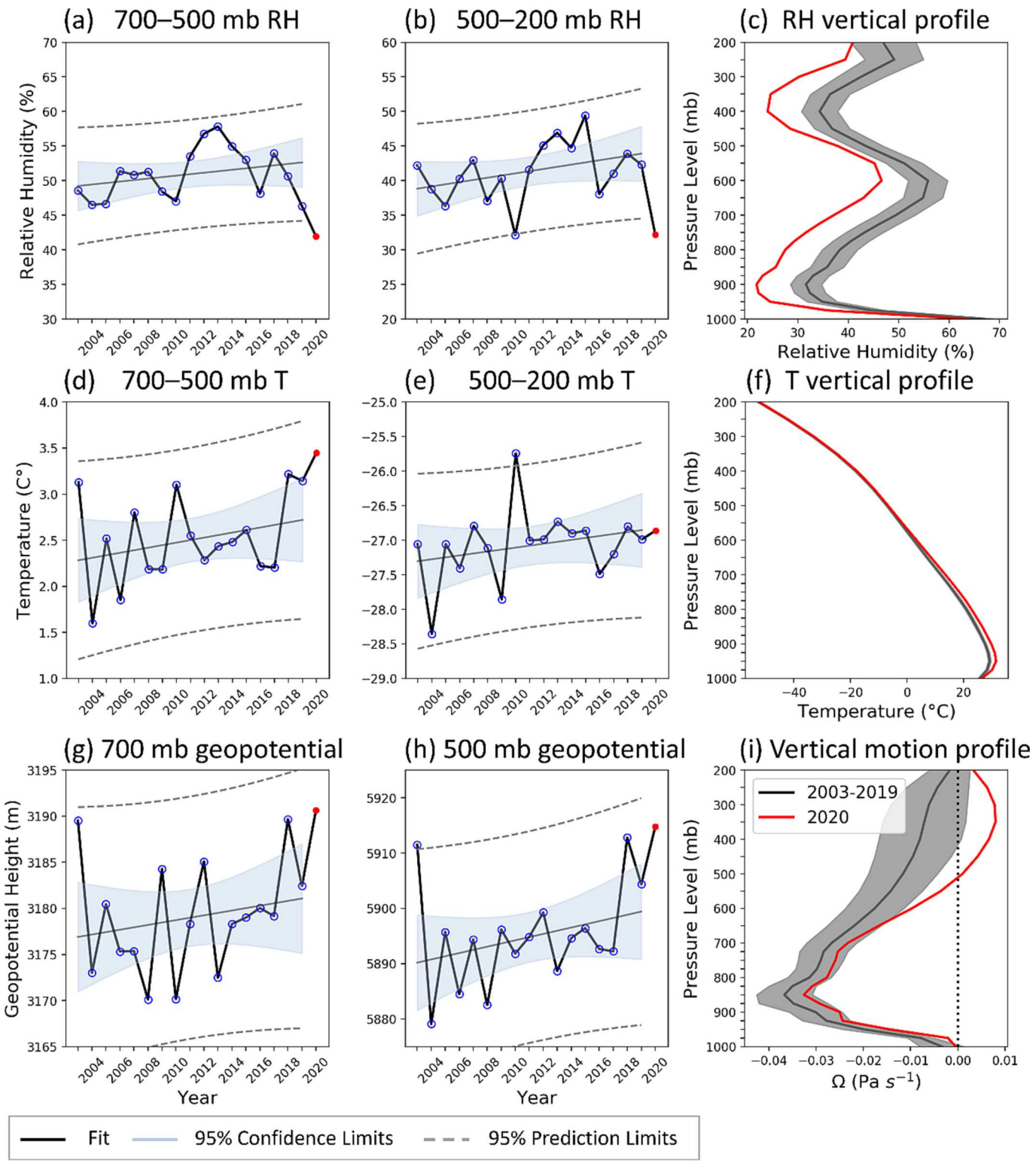

Fig. 6. The time series of April–October layer mean relative humidity (RH) averaged over southwestern US at (a) 700–500 mb, (b) 500–200 mb, and (c) the comparison in RH vertical profile between 2020 (red line) and 2003–2019 mean (black line). (d-f) are similar as (a-c) but for temperature. The time series of mean geopotential height at (g) 700 mb level and (h) 500 mb level. (i) is similar as (c) and (f) but for the comparison of vertical motion. The light blue shading areas in (a-b), (d-e), and (g-h) indicate the 95 % confidence limits, and the black dash line for 95 % prediction limits. All data were generated from MERRA-2. The gray shading in (c), (f), and (i) shows the range of ±1 standard deviation.

more significant role in shaping the radiative effect compared to the influence of cirrus clouds, therefore the changes in CREs over Western Europe during the pandemic cannot be solely attributed to the reduction of AIC. For comparison with Southwestern US, the atmospheric variables over Western Europe are shown in Fig. S7.

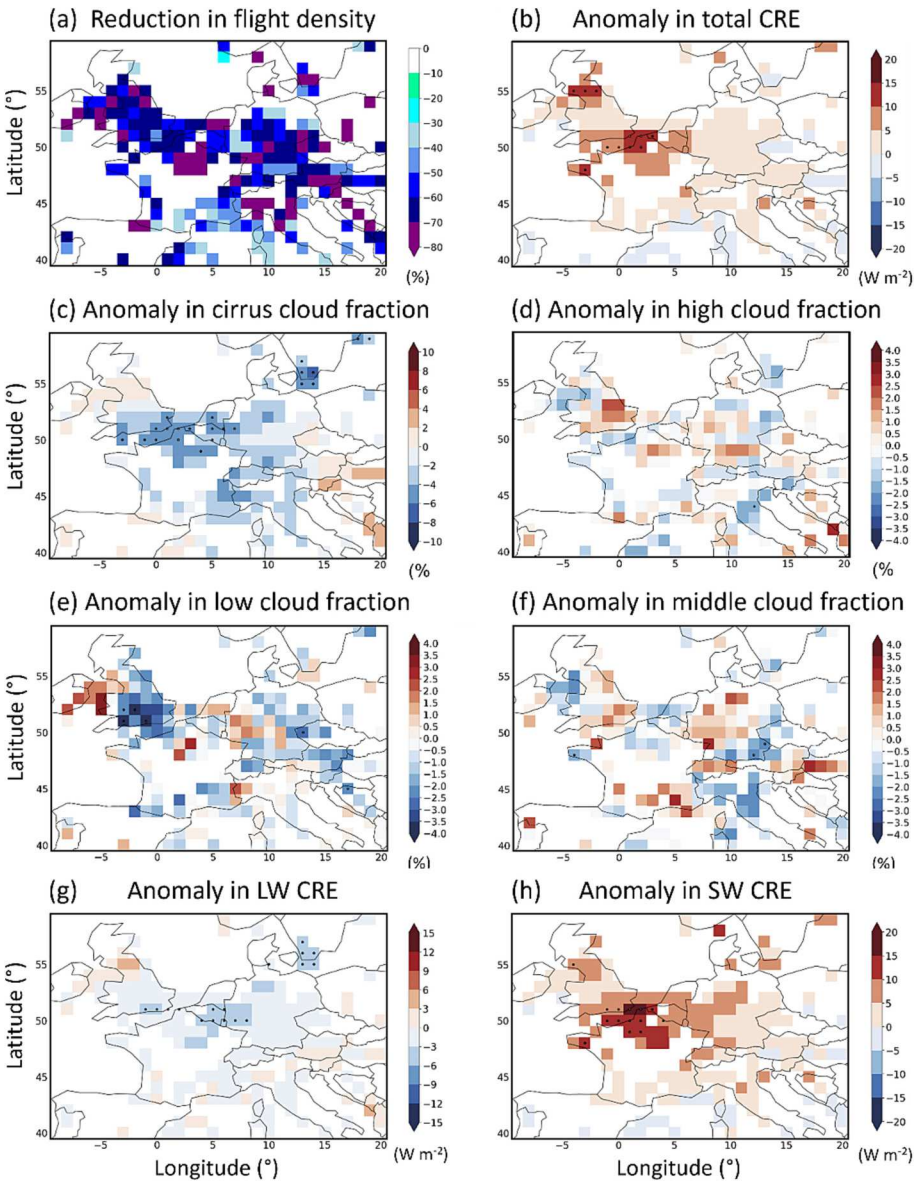

Fig. 7. Same as Fig. 2, but for Western Europe.

4. Conclusions and discussion

AICs have been recognized as one of the most significant anthropogenic atmospheric phenomena that affect the global radiation budget, resulting in substantial alterations in CREs. The global CRE of AICs is projected to increase significantly with the projected increase in air traffic volume, making it crucial to understand their contribution to future climate change. While line-shaped AICs are relatively easy to distinguish from natural cirrus clouds, the quantification of their climatic impact is challenging, mainly because the lack of long-term observational experiment, which bring large uncertainties to the understanding of the underlying mechanisms, as well as the establishment and validation of their parameterization in models.

The COVID-19 pandemic has provided a unique opportunity to examine the climatic impact of contrails. Based on multiple independent satellite observations, a significant decrease in cirrus clouds over the Southwestern United States was detected, causing substantial alterations in both LW and SW CREs, likely due to the reduction in AICs. However, further analyses unravelled that the region also experienced record-setting high pressure and significant low relative humidity during the pandemic period, which made it difficult to separately measure the climatic impact of AICs from natural variability. This highlights the complexity of the atmospheric system and underscores the necessity of further investigation.

Given the projected drastic increase in air traffic volume, AICs could become an important anthropogenic forcing agent by 2050. Therefore, the development of more advanced atmospheric modelling framework that can fully consider the climatic impact of AICs is crucial. This study identifies the location and duration of the most significant disturbance in cloud properties observed during the pandemic. The attribution of these changes to the reduction in AICs or natural variability or other causes and the underlying mechanisms leading to cloud radiative effects remain to be studied using further observations and numerical modelling.

CRediT authorship contribution statement

JW, YL, and XW conceived and designed the study; JW, YL, XW, and YG collected and analyzed the data; JW and YL wrote the manuscript draft; JW, YL, XW, YG, and SY reviewed and edited the manuscript.

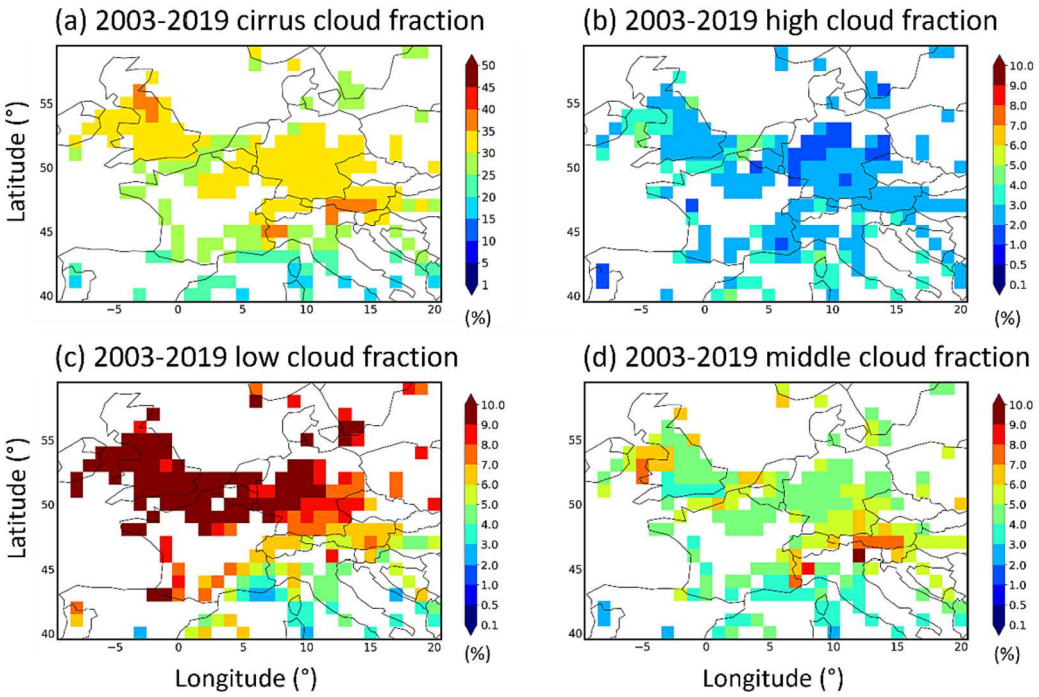

Fig. 8. Same as Fig. 3, but for Western Europe.

Declaration of competing interest

The authors declare that they have no known competing financial interests or personal relationships that could have appeared to influence the work reported in this paper.

Data availability

Data will be made available on request.

Acknowledgement

This study was supported by the Ministry of Education, Singapore, under its Academic Research Fund Tier 1 (RG74/22 to J. W.), Academic Research Fund Tier 2 (MOE-MOET2EP10121-0008 to X. W.), as well as the United States NSF grant AGS-2103820 and NASA ROSES CCST grant (80NSSC23K0119). Y. G. acknowledges the support by (while serving at) the National Science Foundation. The flight statistics data are available at https://www.flightradar24.com/data/statistics. The flight track data are available at https://madis.ncep.noaa.gov/madis_acars.shtml. All Python codes used for data processing and visualization are deposited in a Zenodo repository at https://doi.org/10.5281/zenodo.7795712. The authors declare no conflict of interest. This work comprises Earth Observatory of Singapore contribution No. 558.

Appendix A. Supplementary data

Supplementary data to this article can be found online at https://doi.org/10.1016/j.scitotenv.2023.168656.

References

Bock, L., Burkhardt, U., 2019. Contrail cirrus radiative forcing for future air traffic. Atmos. Chem. Phys. 19, 8163–8174. https://doi.org/10.5194/acp-19-8163-2019.

Bosilovich, M.G., Lucchesi, R., Suarez, M., 2015. MERRA-2: File specification. GMAO Office Note 9 (version 1.0), 73 pp.. Available online at. https://ntrs.nasa.gov/archive/nasa/casi.ntrs.nasa.gov/20150019760.pdf.

Boucher, O., 1999. Air traffic may increase cirrus cloudiness. Nature 397, 30–31. https://doi.org/10.1038/16169.

Boucher, O., et al., 2013. Clouds and aerosols. In: Stocker, T., et al. (Eds.), Climate Change 2013: The Physical Science Basis. Contribution of Working Group I to the Fifth Assessment Report of the Intergovernmental Panel on Climate Change. Cambridge University Press, New York, NY, USA.

Brenguier, J.-L., Burnet, F., Geoffroy, O., 2011. Cloud optical thickness and liquid water path – does the k coefficient vary with droplet concentration? Atmos. Chem. Phys. 11, 9771–9786. https://doi.org/10.5194/acp-11-9771-2011.

Burkhardt, U., Kärcher, B., 2011. Lobal radiative forcing from contrail cirrus. Nat. Clim. Chang. 1, 54–58. https://doi.org/10.1038/nclimate1068.

Castro, C.L., McKee, T.B., Pielke Sr., R.A., 2001. The relationship of the North American Monsoon to tropical and north Pacific sea surface temperatures as revealed by observational analyses. J. Clim. 14, 4449–4472. https://doi.org/10.1175/1520-0442(2001)014<4449:TROTNA>2.0.CO;2.

Castro, C.L., Chang, H., Domiguez, F., Carrillo, C., Schemm, J., Juang, H.H., 2012. Can a regional climate model improve the ability to forecast the North American monsoon? J. Clim. 25, 8212–8237. https://doi.org/10.1175/JCLI-D-11-00441.1.

Chen, Y., 2020. COVID-19 pandemic imperils weather forecast. Geophys. Res. Lett. 47 e2020GL088613.

Digby, R.A.R., Gillett, N.P., Monahan, A.H., Cole, J.N.S., 2021. An observational constraint on aviation-induced cirrus from the COVID-19-induced flight disruption. Geophys. Res. Lett. 48 https://doi.org/10.1029/2021GL095882 e2021GL095882.

Doelling, D., 2019. CERES Energy Balanced and Filled (EBAF) TOA and Surface Monthly Means Data in netCDF Edition 4.1 [Data Set]. NASA Langley Atmospheric Science Data Center DAAC. https://doi.org/10.5067/TERRA-AQUA/CERES/EBAF_L3B.004.1.

Dolinar, E.K., Dong, X., Xi, B., et al., 2019. A global record of single-layered ice cloud properties and associated radiative heating rate profiles from an A-train perspective. Clim. Dyn. 53, 3069–3088. https://doi.org/10.1007/s00382-019-04682-8.

Dong, X., Minnis, P., Ackerman, T.P., Clothiaux, E.E., Mace, G.G., Long, C.N., Liljegren, J. C., 2000. A 25-month database of stratus cloud properties generated from ground-based measurements at the atmospheric radiation measurement southern Great Plains site. J. Geophys. Res. 105 (D4), 4529–4537. https://doi.org/10.1029/1999JD901159.

Dong, X., Xi, B., Wu, P., Dong, X., Xi, B., Wu, P., 2014. Investigation of the diurnal variation of marine boundary layer cloud microphysical properties at the Azores. J. Clim. 27 (23), 8827–8835. https://doi.org/10.1175/JCLI-D-14-00434.1.

Duda, D., Minnis, P., Nguyen, L., 2001. Estimates of cloud radiative forcing in contrail clusters using GOES imagery. J. Geophys. Res. 105, 4927–4937. https://doi.org/10.1029/2000JD900393.

Duda, D.P., Smith, W.L., Bedka, S., Spangenberg, D., Chee, T., Minnis, P., 2023. Impact of COVID-19-related air traffic reductions on the coverage and radiative effects of linear persistent contrails over conterminous United States and surrounding oceanic routes. J. Geophys. Res. Atmos. 128 https://doi.org/10.1029/2022JD037554 e2022JD037554.

Gelaro, R., McCarty, W., Suárez, M.J., Todling, R., Molod, A., Takacs, L., Zhao, B., 2017. The modern-era retrospective analysis for research and applications, version 2 (MERRA-2). J. Clim. 30 (14), 5419–5454. https://doi.org/10.1175/JCLI-D-16-0758.1.

Gettelman, A., Chen, C.-C., Bardeen, C.G., 2021. The climate impact of COVID-19-induced contrail changes. Atmos. Chem. Phys. 21, 9405–9416. https://doi.org/10.5194/acp-21-9405-2021.

Graßl, H., 1990. Possible climatic effects of contrails and additional water vapor. In: Schumann, U. (Ed.), Air Traffic and the Environment - Background, Tendencies and Potential Global Atmospheric Effects. Lecture Notes in Engineering. Springer, Berlin, pp. 124–137.

Hansen, J.E., Travis, L.D., 1974. Light scattering in planetary atmospheres. Space Sci. Rev. 16, 527–610. https://doi.org/10.1007/BF00168069.

Heymsfield, A., Baumgardner, D., DeMott, P., Forster, P., Gierens, K., Kärcher, B., 2010. Contrail microphysics. Bull. Amer. Meteor. Soc. 91, 465–472. https://doi.org/10.1175/2009BAMS2839.1.

Hong, G., Yang, P., Minnis, P., Hu, Y.X., North, G., 2008. Do contrails significantly reduce daily temperature range? Geophys. Res. Lett. 35, L23815.

Horváth, Á., Davies, R., 2007. Comparison of microwave and optical cloud water path estimates from TMI, MODIS, and MISR. J. Geophys. Res. 112, D01202 https://doi.org/10.1029/2006JD007101.

Kärcher, B., 2017. Cirrus clouds and their response to anthropogenic activities. Curr. Clim. Change Rep. 3, 45–57. https://doi.org/10.1007/s40641-017-0060-3.

Kärcher, B., 2018. Formation and radiative forcing of contrail cirrus. Nat. Commun. 9, 1824. https://doi.org/10.1038/s41467-018-04068-0.

Kärcher, B., Burkhardt, U., Ponater, M., Frömming, C., 2010. Importance of representing optical depth variability for estimates of global line-shaped contrail radiative forcing. Proc. Natl. Acad. Sci. U. S. A. 107, 19181–19184. https://doi.org/10.1073/pnas.1005555107.

Karl, T., Koss, W., 1984. Regional and National Monthly, Seasonal, and Annual Temperature Weighted by Area, 1895–1983. Historical Climatology Series 4-3,. National Climatic Data Center, Asheville, NC, 38 pp.

Lee, D.S., Fahey, D.W., Skowron, A., Allen, M.R., Burkhardt, U., Chen, Q., Doherty, S.J., Freeman, S., Forster, P.M., Fuglestvedt, J., Gettelman, A., De León, R.R., Lim, L.L., Lund, M.T., Millar, R.J., Owen, B., Penner, J.E., Pitari, G., Prather, M.J., Sausen, R., Wilcox, L.J., 2021. The contribution of global aviation to anthropogenic climate forcing for 2000 to 2018. Atmos. Environ. 244, 117834 https://doi.org/10.1016/J.ATMOSENV.2020.117834.

Li, Q., Groß, S., 2021. Changes of cirrus cloud properties and occurrence over Europe during the COVID-19-caused air traffic reduction. Atmos. Chem. Phys. 21, 14573–14590. https://acp.copernicus.org/articles/21/14573/2021/.

Liu, Z., Yim, S.H.L., Wang, C., Lau, N.C., 2018. The impact of the aerosol direct radiative forcing on deep convection and air quality in the Pearl River Delta region. Geophys. Res. Lett. 45, 4410–4418. https://doi.org/10.1029/2018GL077517.

Loeb, N.G., Doelling, D.R., Wang, H., Su, W., Nguyen, C., Corbett, J.G., Liang, L., Mitrescu, C., Rose, F.G., Kato, S., 2018. Clouds and the Earth's radiant energy system (CERES) energy balanced and filled (EBAF) top-of-atmosphere (TOA) edition-4.0 data product. J. Clim. 31, 895–918. https://doi.org/10.1175/JCLI-D-17-0208.1.

Mace, G.G., Zhang, Y., Platnick, S., King, M.D., Minnis, P., Yang, P., 2004. Evaluation of cirrus cloud properties derived from MODIS data using cloud properties derived from ground-based observations collected at the ARM SGP site. J. Appl. Meteorol. 44, 221–240.

Marquart, S., Ponater, M., Mager, F., Sausen, R., 2003. Future development of contrail cover, optical depth, and radiative forcing: impacts of increasing air traffic and climate change. J. Clim. 16, 2890–2904. https://doi.org/10.1175/1520-0442(2003)016<2890:FDOCCO>2.0.CO;2.

Matthews, W., Kellogg, W., 1971. In: Robinson, G. (Ed.), Man's Impact on Climate. MIT Press, Cambridge, MA, USA.

Mazon, J.J., Castro, C.L., Adams, D.K., Chang, H.-I., Carrillo, C.M., Brost, J.J., 2016. Objective climatological analysis of extreme weather events in Arizona during the North American Monsoon. J. Appl. Meteorol. Climatol. 55 (11), 2431–2450. https://doi.org/10.1175/JAMC-D-16-0075.1.

Meerkötter, R., Schumann, U., Doelling, D., Minnis, P., Nakajima, T., Tsushima, Y., 1999. Radiative forcing by contrails. Ann. Geophys. 17, 1080–1094. https://doi.org/10.1007/s00585-999-1080-7.

Meijer, V.R., Kulik, L., Eastham, S.D., Allroggen, F., Speth, R.L., Karaman, S., Barrett, S.R. H., 2022. Contrail coverage over the United States before and during the COVID-19 pandemic. Environ. Res. Lett. 17, 034039 https://doi.org/10.1088/1748-9326/ac26f0.

Minnis, P., Young, D., Garber, D., Nguyen, L., Smith, W., Palikonda, R., 1998. Transformation of contrails into cirrus during SUCCESS. Geophys. Res. Lett. 25, 1157–1160. https://doi.org/10.1029/97GL03314.

Minnis, P., Bedka, S., Duda, D., et al., 2013. Linear contrail and contrail cirrus properties determined from satellite data. Geophys. Res. Lett. 40, 3220–3226. https://doi.org/10.1002/grl.50569.

Moroney, C., Menzies, A., DiGirolamo, L., Zhao, G., 2019. Data products specifications for the MISR cloud fraction by altitude product, JPL tech. Doc. D-92238, 12e pp. Available at. https://asdc.larc.nasa.gov/documents/misr/DPS-CFbA.cmm10_24July2019.pdf.

Myhre, G., Stordal, F., 2001. On the tradeoff of the solar and the thermal infrared radiative impact of contrails. Geophys. Res. Lett. 28, 3119–3122. https://doi.org/10.1029/2001GL013193.

Platnick, S., P. Hubanks, K. Meyer, and M. D. King, 2015: MODIS atmosphere L3 monthly product (08_L3). NASA MODIS Adaptive Processing System, Goddard Space Flight Center. doi:https://doi.org/10.5067/MODIS/MYD08_M3.006.

Quaas, J., Gryspeerdt, E., Vautard, R., Boucher, O., 2021. Climate impact of aircraft-induced cirrus assessed from satellite observations before and during COVID-19. Environ. Res. Lett. 16, 064051 https://doi.org/10.1088/1748-9326/abf686.

Schumann, U., 2005. Formation, properties and climate effect of contrails. C. R. Phys. 6, 549–565. https://doi.org/10.1016/j.crhy.2005.05.002.

Schumann, U., Graf, K., 2013. Aviation-induced cirrus and radiation changes at diurnal timescales. J. Geophys. Res. 118 (5), 2404–2421. https://doi.org/10.1002/jgrd.50184.

Schumann, U., Wendling, P., 1990. Determination of contrails from satellite data and observational results. In: Schumann, U. (Ed.), Air Traffic and the Environment - Background, Tendencies and Potential Global Atmospheric Effects. Lecture Notes in Engineering. Springer, Berlin, pp. 138–153.

Schumann, U., Bugliaro, L., Dörnbrack, A., Baumann, R., Voigt, C., 2021a. Aviation contrail cirrus and radiative forcing over Europe during 6 months of COVID-19. Geophys. Res. Lett. 48 (8) https://doi.org/10.1029/2021GL092771 e2021GL092771.

Schumann, U., Poll, I., Teoh, R., Koelle, R., Spinielli, E., Molloy, J., Koudis, G.S., Baumann, R., Bugliaro, L., Stettler, M., Voigt, C., 2021b. Air traffic and contrail changes over Europe during COVID-19: a model study. Atmos. Chem. Phys. 21 (7429–7450), 2021. https://doi.org/10.5194/acp-21-7429-2021.

Spangenberg, D.A., Minnis, P., Bedka, S.T., Palikonda, R., Duda, D.P., Rose, F.G., 2013. Contrail radiative forcing over the northern hemisphere from 2006 Aqua MODIS data. Geophys. Res. Lett. 40, 595–600. https://doi.org/10.1002/grl.50168.

Travis, D., Carleton, A., Lauritsen, R., 2002. Contrails reduce daily temperature range. Nature 418, 601. https://doi.org/10.1038/418601a.

Travis, D.J., Carleton, A.M., Lauritsen, R.G., 2004. Regional variations in U.S. diurnal temperature range for the 11–14 September 2001 aircraft groundings: evidence of jet contrail influence on climate. J. Clim. 17, 1123–1134.

Voigt, C., J. Lelieveld, H. Schlager, J. Schneider, J. Curtius, R. Meerkötter, D. Sauer, L. Bugliaro, B. Bohn, J. N. Crowley, T. Erbertseder, S. Groβ, V. Hahn, Q. Li, M. Mertens, M. L. Pöhlker, A. Pozzer, U. Schumann, L. Tomsche, J. Williams, A. Zahn, M. Andreae, S. Borrmann, T. Bräuer, R. Dörich, A. Dörnbrack, A. Edtbauer, L. Ernle, H. Fischer, A. Giez, M. Granzin, V. Grewe, H. Harder, M. Heinritzi, B. A. Holanda, P. Jöckel, K. Kaiser, O. O. Krüger, J. Lucke, A. Marsing, A. Martin, S. Matthes, C. Pöhlker, U. Pöschl, S. Reifenberg, A. Ringsdorf, M. Scheibe, I. Tadic, M. Zauner-Wieczorek, R. Henke, and M. Rapp (2022). Cleaner skies during the COVID-19 lockdown. Bull. Am. Meteorol. Soc., online, doi.org/10.1175/BAMS-D-21-0012.1.

Wang, Y., Yang, P., Hioki, S., King, M.D., Baum, B.A., Di Girolamo, L., Fu, D., 2019. Ice cloud optical thickness, effective radius, and ice water path inferred from fused MISR and MODIS measurements based on a pixel-level optimal ice particle roughness model. J. Geophys. Res. Atmos. 124, 12126–12140. https://doi.org/10.1029/2019JD030457.

Wilkerson, J., Jacobson, M., Malwitz, A., et al., 2010. Analysis of emission data from global commercial aviation: 2004 and 2006. Atmos. Chem. Phys. 10, 6391–6408. https://doi.org/10.5194/acp-10-6391-2010.

Zhao, L., Wang, Y., Zhao, C., et al., 2022. Compensating errors in cloud radiative and physical properties over the Southern Ocean in the CMIP6 climate models. Adv. Atmos. Sci. 39, 2156–2171. https://doi.org/10.1007/s00376-022-2036-z.

Zhao, Y., Li, J., Zhang, L., Deng, C., Li, Y., Jian, B., Huang, J., 2023. Diurnal cycles of cloud cover and its vertical distribution over the Tibetan plateau revealed by satellite observations, reanalysis datasets, and CMIP6 outputs. Atmos. Chem. Phys. 23, 743–769. https://doi.org/10.5194/acp-23-743-2023.